Cuboplexes: Topologically Active siRNA Delivery

Hojun Kim and Cecilia Leal*

Materials Science and Engineering Department, University of Illinois at Urbana—Champaign, 1304 West Green Street, Urbana, Illinois 61801, United States

ABSTRACT RNAi technology is currently experiencing a revival due to remarkable improvements in efficacy and viability through oligonucleotide chemical manipulations and/or *via* their packaging into nanoscale carriers. At present, there is no FDA-approved system for siRNA technology in humans. The design of the next generation of siRNA carriers requires a deep understanding of how a nanoparticle's physicochemical properties truly impart biological stability and efficiency. For example, we now know that nanoparticles need to be sterically stabilized in order to meet adequate biodistribution profiles. At present, targeting, uptake, and, in particular, endosomal escape are among the most critical challenges impairing RNAi technologies. The disruption of endosomes encompasses membrane transformations (for example, pore formation) that cost significant elastic energy. Nanoparticle size and shape have been identified as relevant parameters impacting tissue accumulation and cellular uptake. In this paper, we demonstrate that the internal structure of lipid-based particles offers a different handle to promote endosomal membrane topological disruptions that enhance siRNA delivery. Specifically, we designed sterically stabilized lipid-based particles that differ from traditional liposomal systems by displaying highly ordered bicontinuous cubic internal structures that can be loaded with large amounts of siRNA. This system differs from traditional siRNA-containing liposomes (lipoplexes) as the particle—endosomal membrane interactions are controlled by elasticity energetics and not by electrostatics. The resulting "PEGylated cuboplex" has the ability to deliver siRNA and specifically knockdown genes with efficiencies that surpass those achieved by traditional lipoplex systems.

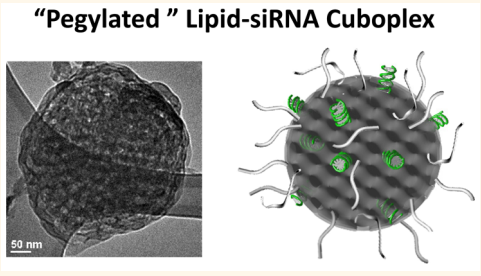

KEYWORDS: cubosomes · siRNA delivery · nanoparticles · bicontinuous cubic phases · liposomes · PEGylated liposomes · nanomedicine

The delivery of encapsulated exogenous drugs or genes to cells is a challenge that for decades has motivated the development of numerous delivery nanoparticles with diverse chemical and physical properties.[1−7] The general design principles for particulate materials intended for cellular delivery need to attain a number of challenging requirements: colloidal stability, superior encapsulation power, resilience in the circulation system, low cytotoxicity, specificity to the target site, as well as optimal tissue penetration and clearance pathways. Investigating the optimal size of nanoparticles has been the prime focus of designing cellular delivery systems.[8] In addition to size, the shape of nanoparticles has been recently identified as a handle to control cellular uptake rates and mechanisms.[9−13] Mitragotri *et al.* reported that the co-delivery of anticancer drugs through shape-engineered polymer-based vehicles shows inhibitory concentrations of anticancer drugs up to 10 000-fold lower than that of individual drugs.[14] For lipid-based nanoparticles, Olvera de la Cruz and coworkers recently demonstrated that controlling the membrane structure properties is a fruitful route for obtaining specific particulate shapes.[12,15−17] In this work, we used a new class of soft lipid particles loaded with small interfering RNA (siRNA) to demonstrate for the first time that particle internal structure has a crucial role in cellular delivery efficiency.

RNA interference (RNAi) therapy that can be achieved by the cytoplasmic delivery of siRNA leading to specific gene knockdown[18−21] has recently experienced a revival[22] due to remarkable improvements in potency and stability through chemical modification of the oligonucleotides themselves or through their packaging into nanoparticles, such as cationic liposomes. A specific example is the recent finding that siRNAs encapsulated in lipid-nanoparticles rapidly adapted to target Ebola viruses, protecting 100% of rhesus monkeys against lethal fate.[23]

While some pharmaceutical companies are opting for the cellular delivery of naked

* Address correspondence to cecilial@illinois.edu.

Received for review June 25, 2015 and accepted September 21, 2015.

Published online September 21, 2015
10.1021/acsnano.5b03902

siRNA as a simple and less costly approach for local treatments in the eye and lung, the majority of the advances have been realized after refinement of encapsulation technologies based on lipid or polymer formulations. Finding the optimal lipid constituents and their relative composition that can effectively encapsulate and deliver siRNA to organs in a systematic manner is still, to a large extent, an empirical process.

The translation from *in vitro* to *in vivo* RNAi therapy has been the focus of many important developments,[24−27] but few attempts have succeeded to reach clinical trials,[28] mostly due to poor cell penetration and low durability of effects.[29] The state of the art challenges in siRNA technology were recently reviewed by Yin and co-workers.[20] While the encapsulation of siRNA into nanoparticles ensures its protection from serum endonucleases and immune recognition,[30] the interaction between the delivery system and serum constituents can impair their function. Lipid nanoparticles need to be positively charged to electrostatically trap siRNA, and a certain membrane charge density threshold has been identified as a requirement to ensure efficient endosomal escape.[31] However, particles' surface charge will affect their aggregation behavior as well as the adsorption of serum proteins during circulation. In particular, some nanoparticles can be disrupted when interacting with the negatively charged glomerular basement membranes,[32,33] resulting in the urine clearance of siRNA. Lipid nanoparticle aggregation and surface interactions can be modulated by the addition of polyethylene glycol conjugated[34,35] lipids ("PEGylated" nanoparticles), resulting in effective biodistribution and circulation times *in vivo*. Crucial barriers to consider when designing siRNA delivery nanoparticles are cellular uptake and efficient release into the cytoplasm. The main pathway for siRNA−nanoparticle delivery to the cell is *via* endocytosis, and nanoparticles have been designed to incorporate ligands that bind to receptors that activate endocytosis to enhance cell entry rate.[36] However, endocytosed nanoparticles must be able to escape endosomal entrapment before maturation of acidic late endosomes in addition to resisting clearance *via* endocytic recycling and exocytosis.[37] Clearly, controlling nanoparticle surface properties and endosomal release is vital for nanoparticle design for efficient siRNA encapsulation and delivery.

Leal and co-workers[38,39] established that the use of nonlamellar lipid complexes containing siRNA, in particular, the use of a bulk bicontinuous gyroid phase based on glycerol monooleate (GMO) and small amounts of positively charged lipids, displayed superior performance for siRNA delivery and specific knockdown in mammalian cell culture when compared to parent lipoplex systems having the classic stacked bilayer architecture. Analogously, we recently demonstrated that ultrasound-triggered drug release from classical liposomal systems is activated through tensions in the lipid membrane toward the stabilization of non-bilayer phases.[40] The main argument for the gene-silencing efficiency enabled by the bicontinuous gyroid phase was that such lipid complexes do not rely on electrostatic-mediated fusion with endosomal membranes and instead are "topologically" active, lowering the free energy required to promote fusion and pore formation, with the endosomal membrane leading to efficient escape. This was an important finding toward the development of siRNA delivery systems that are required to comprise low contents of positive charges while being efficient to escape endosomal entrapment. However, the system used in this former study was in a bulk state without colloidal stability; the size of the complexes was exceeding several microns, and PEGylated moieties were absent. In other words, while adequate for cell culture studies, such material would not be appropriate for a systemic administration that requires a stable nanoscale particulate system. In this paper, we demonstrate our approach to generate, for the first time, PEGylated colloidally stable nanoparticles with high siRNA encapsulation power, containing low contents of positively charged species, and with the unique characteristic of having a highly ordered bicontinuous internal structure that results in topological-driven endosomal escape for efficient siRNA delivery.

RESULTS AND DISCUSSION

Our study focuses on the design of siRNA delivery vehicles with internal structure, colloidal stability, as well as PEGylated surfaces. In order to accomplish this goal, we designed the lipid composition to comprise a bicontinuous cubic phase forming lipid glycerol monooleate (1-monooleyl glycerol), a net positively charged lipid 1,2-dioleoyl-3-trimethylammonium propane (DOTAP) commonly used in nucleic acid delivery[41] for siRNA electrostatic pinning and favorable interaction with negatively charged cell membranes, and a custom-designed GMO lipid conjugated to 2 kDa polyethylene glycol (GMO-PEG). This molecule is a neat PEGylated monoolein that contrasts analogous molecules in the literature[42] by not having the unnecessary covalently linked NHS derivative. We hypothesized that there will be an optimum ratio of where these three different lipids will allow the formation of PEGylated bicontinuous cubic phase particulates for enhanced endosomal escape and optimal biodistribution and circulation times. Lipid-based particles with internal bicontinuous cubic symmetry, the so-called cubosomes, were first described by Larsson in 1989.[43−52] The preparation of these particles requires the addition of stabilizing polymer solutions combined with very high temperature homogenization, which impairs the bottom-up encapsulation of biological

molecules. Recently, Martiel and co-workers suggested an alternative method to prepare sub-micron-sized structured lyotropic particles with a significantly reduced energy input by evaporation of an auxiliary volatile solvent immiscible with water, where the inner structure of the particles could be regulated by the addition of a nonvolatile oil.[53] In this work, we suggest an approach where exclusively the lipid components of the particles are required in combination with ultrachilled indirect low-power sonication. siRNA can be encapsulated during the bottom-up hydration process analogous to a classical liposome production. We describe a combination of methods: (i) small-angle X-ray scattering, (ii) fluorescence optical microscopy, (iii) cryogenic transmission electron microscopy, and (iv) cell culture gene knockdown to underpin the key concepts in designing PEGylated topologically active siRNA lipid carriers and to demonstrate for the first time that, aside from nanoparticle shape and size, internal structure has a determining role in efficient cellular delivery.

Small-Angle X-ray Scattering (SAXS). In this work, we used SAXS to systematically investigate the particle design space in terms of how a GMO-based cubic structure evolves with increasing amounts of added charged and colloidally stabilizing lipids with and without the presence of siRNA.

Figure 1A displays the integrated SAXS data obtained for a ternary mixture of GMO/DOTAP/GMO-PEG at fixed GMO-PEG composition (molar fraction: $\Phi_{GMO\text{-}PEG} = 0.02$) as a function of increasing amounts of DOTAP (Φ_{DOTAP}). Increasing DOTAP content from $\Phi_{DOTAP} = 0.01$ to $\Phi_{DOTAP} = 0.98$ leads to the stabilization of three distinct equilibrium phases (two bicontinuous cubic phases and one lamellar phase). At low DOTAP composition (GMO/DOTAP/GMO-PEG (97/1/2)) with $\Phi_{DOTAP} = 0.01$, seven sharp peaks are found, at the reciprocal lattice vectors $q/(2\pi/a) = G_{hkl}/(2\pi/a) = (h^2 + k^2 + l^2)^{1/2} = \sqrt{2}, \sqrt{4}, \sqrt{6}, \sqrt{10}, \sqrt{12}, \sqrt{14}, \sqrt{18}$ corresponding to the [110], [200], [211], [310], [222], [321], and [411] reflections, respectively. These reflections are matched with a primitive 3D bicontinuous cubic structure with lattice spacing $a^{Q_{II}^P} = 186.7$ Å (space group *Im*3*m*, labeled Q_{II}^P). The peak indexes are completely satisfying the Q_{II}^P structure rules: (i) $(h + k + l) = 2n$, (ii) $0kl$ $(k + l = 2n)$, (iii) hhl $(l = 2n)$, (iv) $h00$ $(h = 2n)$, (v) hkl (k, l = $2n$) (with h, k, l permutable and n is an integer).[54] For pure GMO/water systems, one is accustomed to encounter bicontinuous cubic phases with either diamond *Pn*3*m* or gyroid *Ia*3*d* symmetry, depending on water content.[55] However, the inclusion of rather small, modified GMO lipid content with bulky head groups leads to the stabilization of the primitive *Im*3*m* bicontinuous cubic phases. This is observed, for example, in binary mixtures of GMO/GMO-Gd_DTPA (98/2 mol %).[56] For the cases studied in this paper, a bulky GMO-PEG is included in all materials, and we found an analogous behavior. The addition of as little as 1 mol % of PEGylated GMO to a pure GMO system

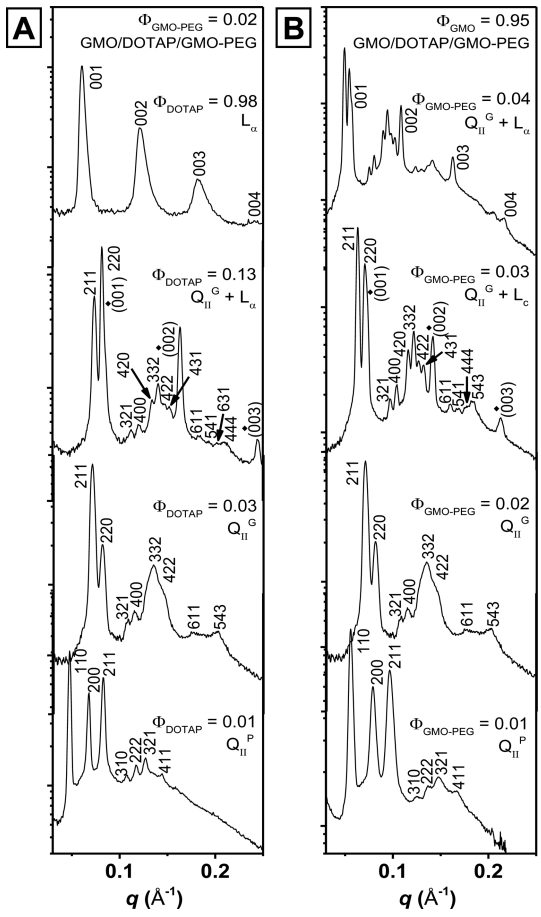

Figure 1. SAXS data obtained for the ternary mixture of GMO/DOTAP/GMO-PEG. (A) SAXS scans obtained for increasing amounts of DOTAP molar fractions (Φ_{DOTAP}) at fixed GMO-PEG composition ($\Phi_{GMO\text{-}PEG} = 0.02$). At the lowest DOTAP composition ($\Phi_{DOTAP} = 0.01$), seven intense Bragg peaks are observed. These seven Bragg reflections are successfully matched with a primitive-type bicontinuous cubic phase with the space group *Im*3*m* (termed Q_{II}^P) with unit cell dimensions of a = 159.5 Å. SAXS scans at $\Phi_{DOTAP} = 0.03$ display eight distinct Bragg peaks, which are consistent with a body-centered bicontinuous gyroid cubic structure with the space group *Ia*3*d* (termed Q_{II}^G) with a = 217 Å. At $\Phi_{DOTAP} = 0.13$, SAXS scans reveal a coexistence of Q_{II}^G and another phase that is matched to a classical lamellar phase (L_α) with its repeating distance $d = 2\pi/q_{001} = 77.1$ Å. At far larger DOTAP contents, the system transitions to a pure L_α phase with d = 128.8 Å. We believe that this phase evolution as a function of DOTAP composition is attributed to repulsive charge interactions in the lipid aggregates. (B) SAXS scans obtained for increasing amounts of GMO-PEG molar fractions ($\Phi_{GMO\text{-}PEG}$) at fixed GMO composition ($\Phi_{GMO} = 0.95$). At the lowest content of GMO-PEG, $\Phi_{GMO\text{-}PEG} = 0.01$, seven sharp peaks are successfully indexed to the bicontinuous cubic *Im*3*m* phase (Q_{II}^P), a = 160 Å. As $\Phi_{GMO\text{-}PEG}$ increases, the SAXS scans reveal that the *Im*3*m* cubic phase was completely transformed to another structure that can be perfectly matched to the gyroid *Ia*3*d* cubic phase at $\Phi_{GMO\text{-}PEG} = 0.02$, a = 217 Å. At $\Phi_{GMO\text{-}PEG} = 0.03$, the SAXS scans indicate that the system evolves into the equilibrium of two different phases, Q_{II}^G and L_α. Further increase of GMO-PEG contents ($\Phi_{GMO\text{-}PEG}$ = 0.04) increases the fraction of the L_α phase. In this case, the phase behavior of the system is driven by the large hydration pulling of the PEG domains in GMO-PEG.

leads to a $Pn3m \rightarrow Im3m$ phase transition as described in Supporting Information Figure S1. Increasing the amount of GMO-PEG from 1 to 2 mol % results in an expansion of the lattice spacing of the *Im3m* cubic unit cell.

When the amount of DOTAP is increased to $\Phi_{DOTAP} = 0.03$, a second phase was obtained and eight sharp peaks are observed at $q/(2\pi/a) = G_{hkl}/(2\pi/a) = (h^2 + k^2 + l^2)^{1/2} = \sqrt{6}, \sqrt{8}, \sqrt{14}, \sqrt{16}, \sqrt{22}, \sqrt{24}, \sqrt{38}$, and $\sqrt{50}$ corresponding to the reflections of [211], [220], [321], [400], [332], [422], [611], and [543]. Except for a few reflections that are convoluted with higher intensity peaks, all of the peaks are matched with a body-centered gyroid cubic structure with the space group *Ia3d*, with $a^{Q_{II}^G} = 217$ Å (labeled Q_{II}^G). The peak indexes are completely satisfying the Q_{II}^G structure rules: (i) $(h + k + l) = 2n$, (ii) $0kl$ $(k, l = 2n)$, (iii) hhl $(2h + l = 4n)$, and (iv) $h00$ $(h = 4n)$ (with h, k, l permutable and n is an integer). When the DOTAP composition increases to $\Phi_{DOTAP} = 0.13$, another phase emerges in coexistence with the *Ia3d*. This phase is assigned to a classic lamellar structure of lipid bilayers (L_α) with three Bragg reflections observed at $q_{001} = 0.082$ Å^{-1}, $q_{002} = 0.16$ Å^{-1}, and $q_{003} = 0.24$ Å^{-1} and a corresponding lattice spacing of $a^{L_\alpha} = 77.1$ Å. Interestingly, an inverse hexagonal phase that has been obtained for GMO/DOTAP binary systems[38] was not observed here for the ternary GMO/DOTAP/GMO-PEG mixture at any composition. Instead, as the amount of DOTAP increased, the system switches from the cubic phase directly into a lamellar configuration. The bulky nature of the PEG unit (2 kDa) of the PEGylated GMO lipid might be hard to stabilize in 2D hexagonal systems of the reverse-type, where water tubes are roughly just 5 nm in diameter.

In order to understand how the addition of the PEGylated GMO-PEG lipid modulates the GMO-based cubic phase behavior, we fixed GMO at 95 mol % and varied GMO-PEG content of the GMO/DOTAP/GMO-PEG ternary mixture. We observed that very small increments of added GMO-PEG (1 mol %) have a dramatic impact on the phase behavior. Figure 1B shows the SAXS scans obtained for a system at $\Phi_{GMO} = 0.95$. The addition of 1 mol % of GMO-PEG yields a well-ordered Q_{II}^P phase. However, at 2 mol % of GMO-PEG, the Q_{II}^P is transformed into the Q_{II}^G. The lattice spacing of the Q_{II}^P phase is considerably smaller than that in the Q_{II}^G phase ($a^{Q_{II}^P} = 160$ Å and $a^{Q_{II}^G} = 217$ Å). The inclusion of GMO-PEG with a bulky PEG unit pushes the unit cell of the Q_{II}^P phase to expand and eventually induce the phase transformation toward the Q_{II}^G phase. As the GMO-PEG composition increases, a lamellar phase (L_α) emerges in coexistence with bicontinuous cubic gyroid (Q_{II}^G). Here, the steric effect of GMO-PEG addition was also observed with the lattice spacing increasing from $a^{Q_{II}^G} = 217$ Å at $\Phi_{GMO\text{-}PEG} = 0.02$ to 245 Å, at $\Phi_{GMO\text{-}PEG} = 0.03$, and eventually $a^{Q_{II}^G} = 313$ Å at $\Phi_{GMO\text{-}PEG} = 0.04$. It is remarkable that the bicontinuous gyroid cubic lattice spacing can increase by 100 Å while retaining crystalline order by the addition of rather small amounts of PEGylated lipids. We believe that this lattice expansion is associated with an augmented degree of swelling driven by osmotic pulling of the PEG moieties. Lattice expansion due to higher swelling of lipid gyroids was observed in the past by the addition of charged lipids, but the lattice spacings in that case did not exceed 200 Å.[38,57] Recently, a number of methods including the addition of cholesterol in combination with charged lipids have been utilized in order to expand the swelling capacity of lipid cubic phases up to 470 Å.[58] This is an indication that in addition to Coulomb repulsions (*via* charged lipids addition) the combined effects of electrostatics and membrane elasticity using cholesterol and/or PEGylated lipids offer another handle to control cubic phase unit cell dimensions.

There are common phase behavior features between adding DOTAP and GMO-PEG to GMO-based systems. In both cases, there is an expansion of the bicontinuous cubic unit cell, which is expected due to electrostatic repulsion-driven swelling (DOTAP)[57] or due to osmotic water pulling (GMO-PEG). Interestingly, the swelling of the bicontinuous cubic phase is accompanied also by a structural change from the *Im3m* to an *Ia3d* symmetry group. A relevant difference between these two cubic phases is the total surface area, with the *Ia3d* phase having a surface area higher than that of the *Im3m* phase.[59] At this point, the driving force of the phase transition cannot be decisively underpinned, but the indication is that electrostatic repulsion between DOTAP-charged head groups or the bulky PEGylated lipids (which also results in increased areas per lipid head groups) seems to have a preference to be organized in a cubic phase geometry where there is larger bilayer surface areas.

The results explained above indicate that there are two prime compositions that allow the stabilization of two bicontinuous cubic phases of distinct symmetry (*Im3m* and *Ia3d*) containing a ternary mixture of GMO/DOTAP/GMO-PEG lipids. The *Ia3d* phase was previously identified for binary GMO/DOTAP mixtures, where siRNA could be completely incorporated without disruption of the structure. In this work, we investigate to what extent siRNA can be incorporated in the two cubic phases of distinct symmetry now for the ternary lipid system. Figure 2A shows the SAXS scans obtained for GMO/DOTAP/GMO-PEG (95/4/1), displaying the bicontinuous primitive cubic structure for the lipid-only system (black line, $Q_{II}^{P,lipids}$) and for a system with added siRNA at fixed charge ratio ρ (n_{DOTAP}/n_{NA}) = 1 (red line, $Q_{II}^{P,siRNA}$). Here, the charge ratio ρ is defined as the ratio of number of positive charges per lipid molecules (n_{DOTAP}) over the number of negative charges per siRNA (n_{NA}). The system containing siRNA

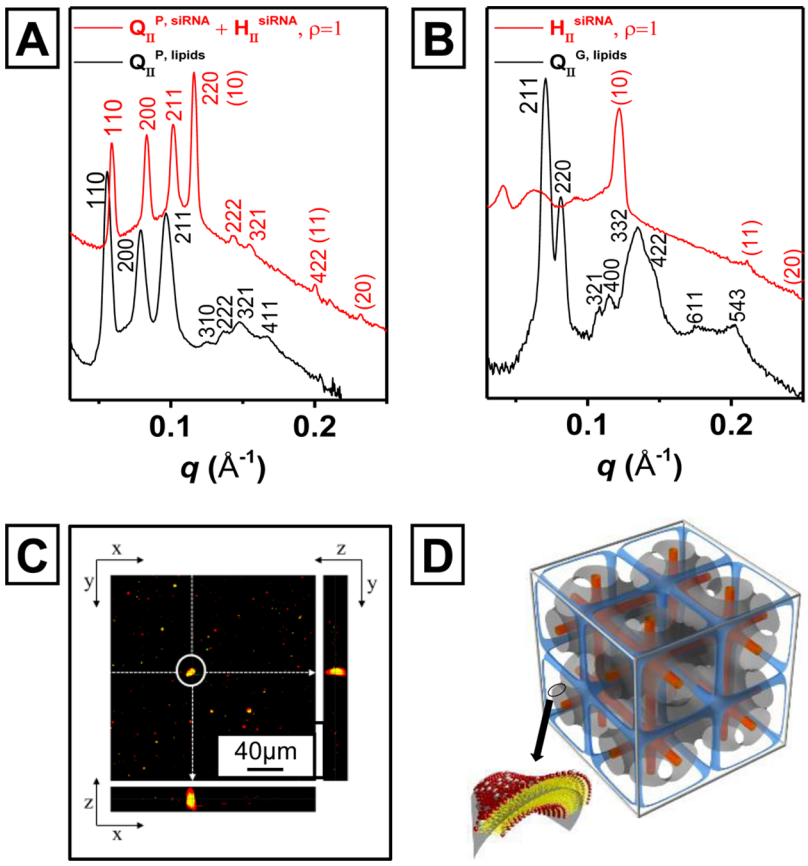

Figure 2. Effect of siRNA inclusion into the bicontinuous cubic phases of *Im*3*m* and *Ia*3*d* symmetry. (A) SAXS scans obtained for the GMO/DOTAP/GMO-PEG (95/4/1) lipid-only *Im*3*m* cubic phase (black line) and its corresponding GMO/DOTAP/GMOPEG−siRNA phase in the regime of charge neutrality ρ (n_{DOTAP}/n_{NA}) = 1 (red line). The SAXS data of the lipid-only system correspond to the bicontinuous cubic *Im*3*m* ($Q_{II}^{P,lipids}$) phase with a unit cell of $a^{Q_{II}^{P,lipids}}$ = 159.5 Å. Incorporating siRNA into this phase results in a SAXS profile (red line) that is consistent with the conservation of the same bicontinuous cubic phase ($Q_{II}^{P,siRNA}$) but at smaller unit cell dimensions due to siRNA screening of DOTAP electrostatic repulsion, $a^{Q_{II}^{P,siRNA}}$ = 150.6 Å. A residual amount of a coexisting phase can be seen by the presence of three overlapping SAXS peaks that can be indexed to a 2D reversed hexagonal phase (H_{II}^{siRNA}): (10), (11), and (20), with a unit cell dimension of *a* = 59.5 Å. Cubic phases tend to transform into hexagonal phases upon nucleic acid inclusion,[38,61] but in this case, it is noteworthy that the majority of the observed phase is still the bicontinuous cubic *Im*3*m* ($Q_{II}^{P,siRNA}$). (B) SAXS scans obtained for the GMO/DOTAP/GMO-PEG (95/3/2) lipid-only *Ia*3*d* cubic phase (black line) and its corresponding GMO/DOTAP/GMO-PEG (95/3/2)−siRNA phase ρ = 1 (red line). The SAXS data acquired for the lipid-only system correspond to the bicontinuous cubic *Ia*3*d* ($Q_{II}^{G,lipids}$) phase with a unit cell of $a^{Q_{II}^{P,lipids}}$ = 217 Å. When siRNA is added to the well-ordered *Ia*3*d* phase, the SAXS scans reveal that the cubic structure is transformed into a dominant H_{II}^{siRNA} with a unit cell dimension of *a* = 59.5 Å. The gyroid *Ia*3*d* phase is less flexible to siRNA encapsulation than the *Im*3*m* cubic structure. (C) Confocal microscopy image of the *Im*3*m* cubic phase containing siRNA GMO/DOTAP/GMO-PEG (95/4/1)−siRNA at ρ = 1. The lipid components are tagged with a red fluorescent dye DHPE-Texas Red and siRNA with green YoYo-1. Domains where lipid and siRNA are completely colocalized should appear yellow. The confocal microscopy image clearly indicates that in large lipid−siRNA aggregates the lipid and siRNA domains are completely colocalized in three dimensions, as evidenced by the *ZY* and *ZX* planes plotted adjacent to the large *XY* image slice. (D) Schematic illustration of the unit cell structure of a bicontinuous cubic *Im*3*m* phase (Q_{II}^{P}). The midplane of the lipid membrane is represented as a gray surface, which separates two intertwined but independent aqueous nanochannels (indicated with orange and blue).

displays the same bicontinuous cubic structure as the parent lipid system, except that there is a significant reduction (5.6%) of the lattice spacing ($a^{Q_{II}^{P,lipids}}$ = 159.5 Å and $a^{Q_{II}^{P,siRNA}}$ = 150.6 Å), an observation that is common when nucleic acids are able to screen the charge repulsion of positively charged lipid membranes containing DOTAP.[60] To our knowledge, this is the first time that a PEGylated lipid bicontinuous cubic phase containing siRNA is reported. A suspiciously strong (220) reflection indicates that the cubic phase might be in equilibrium with a residual inverse hexagonal phase H_{II}^{siRNA} with an overlapped (10) reflection followed by the corresponding (11) and (20) reflections. The relative amount of hexagonal phase coexistence can be modulated by adding increasing amounts of DOTAP (cf. Figure S2). Pure cubic phases containing nucleic acids have proven to be rather difficult to stabilize, and in most instances, the system evolves to a pure hexagonal phase.[61,62] In fact, most cubic phase hosts reported in the literature are used to encapsulate and/or crystallize rather small globular protein molecules.[42,63,64]

In Figure 2B, we show the SAXS scans obtained for GMO/DOTAP/GMO-PEG (95/3/2) without (black line)

and with (red line) siRNA incorporation. In this case, the bicontinuous cubic gyroid phase ($Q_{II}^{G,lipids}$) obtained for lipids alone is transformed entirely into an inverse hexagonal phase (H_{II}^{siRNA}). Three Bragg peaks at q_{10} = 0.122 Å^{-1}, q_{11} = 0.211 Å^{-1}, and q_{20} = 0.243 Å^{-1} are consistent with a 2D hexagonal phase with a lattice spacing of a = 59.5 Å ($a = (4\pi)/(q_{10}\sqrt{3})$). Interestingly, for the lipid-only ternary systems containing PEGylated units, a reversed hexagonal phase was not found in a rather careful compositional investigation, but the inclusion of siRNA allows the stabilization of this phase. First, this is an indication that siRNA is indeed included in the lipid matrix phase.[61] In addition, in a reversed hexagonal phase, siRNA occupies the water domain with the lipids decorating the nucleic acid. In this arrangement, the bulky PEGylated units can be displaced out of the water domain into stabilizing the oily/water interface of the lipid−siRNA complex. Real space imaging shown later in this paper indicates that this might be, in fact, the case.

It is noteworthy that, in contrast to the GMO/DOTAP-siRNA system[38] where the gyroid was the lowest energy cubic phase, when small amounts of PEGylated GMO is added to the system, *Im*3*m* is the preferred bicontinuous cubic phase. Infinite periodic minimal surfaces have an infinite *genus*, but per unit cell, this is defined and determined by the number of topologically distinct holes per unit cell. For the *Im*3*m* and *Ia*3*d* phases, the genus of the minimal surfaces per unit cell is the same because they are connected by the Gauss-Bonnet transformation.[59] In this context, a more useful parameter to distinguish both phases is a_0, a dimensionless area per unit cell of the cubic phase, which has the values 2.345 and 3.091 for the primitive and the gyroid underlying minimal surfaces of the *Im*3*m* and *Ia*3*d* phase, respectively. This allows us to calculate the total area of a certain cubic phase A by equaling it to a^2a_0, where a is the regular lattice spacing of the cubic phase. For the present systems, that equates to A^{Im3m} = 592.7 nm^2 *versus* A^{Ia3d} = 1455 nm^2. In other words, the surface area of the *Ia*3*d* cubic gyroid phase is substantially higher than that of the *Im*3*m* primitive bicontinuous cubic phase, which means that membranes in a gyroid will have more folded/curved regions in the 3D space. In this regard, the incorporation of oppositely charged stiff nucleic acids molecules, which is known to promote transitions to lipid phases with flatter lipid films,[61] will be more favorable in a membrane with a lower degree of curved space such as that of the *Im*3*m* cubic phase. The water channel diameters were calculated[65] as 4.9 and 5.9 nm for the *Im*3*m* and *Ia*3*d* phases, respectively, dimensions which are perfectly suited to incorporate siRNA molecules that have a molecular diameter of 2.6 nm.

Confocal Microscopy. In order to evaluate the extent of siRNA encapsulation within the new PEGylated bicontinuous primitive lipid cubic phase, we conducted confocal microscopy to investigate the colocalization of the lipid and siRNA domains. We used a fluorescent red lipid tag molecule, Texas Red conjugated lipid, and a siRNA binding green fluorescent tag YoYo-1. The confocal microscopy image of stoichiometrically charge-neutral lipid−siRNA complexes ($\rho = 1$) is shown in Figure 2C. The central panel is an *XY* image slice displaying a few yellow aggregates of about 10 μm, clearly showing that siRNA (green) and lipid (red) domains are totally colocalized. The *ZY* and *ZX* side images also demonstrate that the colocalization of siRNA and lipid domains remains throughout the entire 3D thickness of the lipid−siRNA complex aggregates. A schematic representation of the structure of the Q_{II}^{P} bulk cubic phase is represented in Figure 2D. A lipid membrane with the midplane represented in gray is a periodic minimal surface that separates two intertwined but independent aqueous nanochannels (represented by orange and blue) organized with *Im*3*m* cubic symmetry.

Cryogenic Transmission Electron Microscopy (Cryo-TEM). The application of the cubic phase intended for systemic cellular delivery applications requires the production of a colloidally stable particulate system. In this work, we demonstrate that a judicious choice of lipids allows the preparation of PEGylated nanoparticles by gentle indirect sonication at low temperatures with internal structures that are conserved from the original bulk cubic phase. The fragmentation of the bulk cubic phase results in the production of micron-sized particles within 6 min of chilled indirect sonication (cf. Figure S3), and a total time of 10 min is sufficient for the production of nanoparticles on the order of 500 nm. The average size of the cubosome particles as determined by dynamic light scattering (Table S1) is rather constant over time (*ca.* 300 nm) even in the absence of PEGylated lipids due to the presence of cationic species (DOTAP) conferring an electrostatic stabilization. Adding GMO-PEG components leads to an extended temporal stabilization of particle size, although the main function of PEGylated lipid inclusion relates to the fact that these species are known to improve particle circulation time for *in vivo* applications. It is noteworthy that our method of dispersing particles is suitable for the preparation of PEGylated cubosomes with and without siRNA (90% encapsulation efficiency); we refer to the latter type of nanoparticles as *cuboplexes*. While SAXS is a critical tool to identify the nanostructure of the bulk aggregates, the structures of dilute solutions of nanoparticles are most appropriately assessed by cryo-TEM, where the sample is quickly quenched at ultralow temperatures and the nanoscale objects can be observed as in their native solution state. Cryo-TEM is the technique of choice when investigating the structure of lipid-based suspensions, including those containing drugs and nucleic acids.[66] In the case of lipid phases other than the

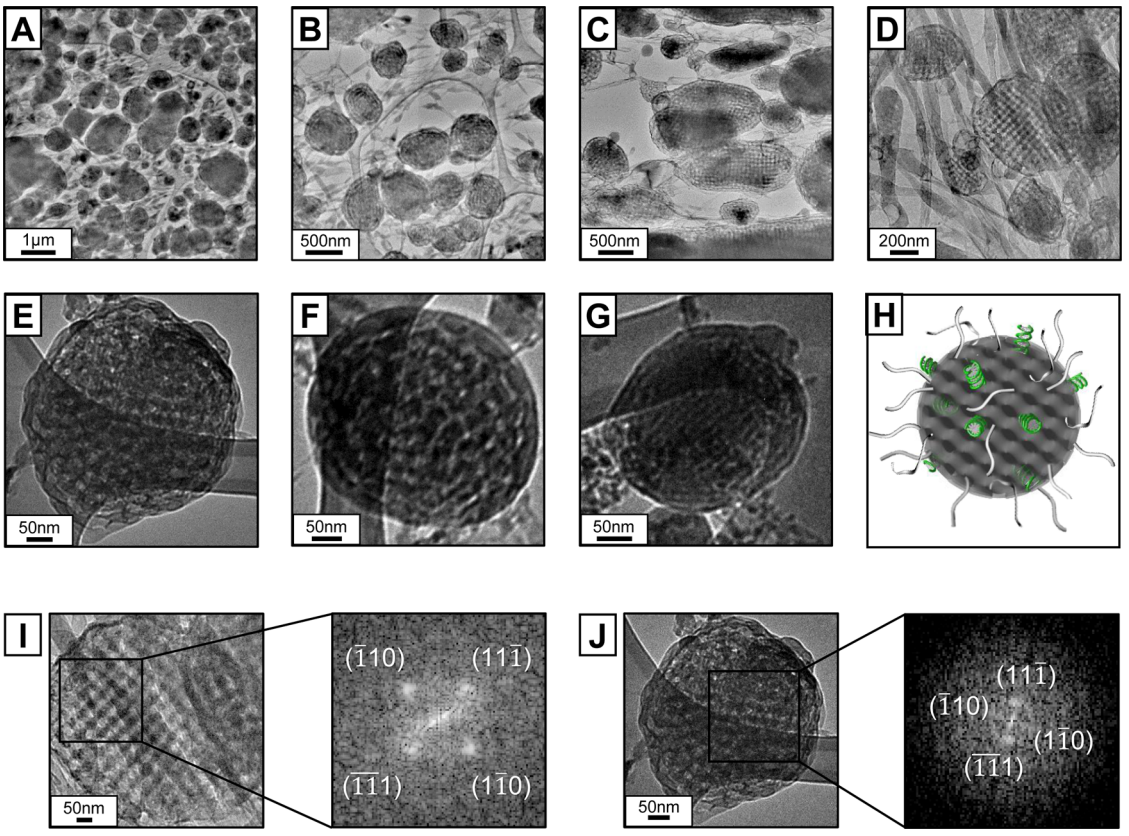

Figure 3. Cryo-TEM study of lipid-only and lipid−siRNA *Im3m* cubic phases fragmented into nanoparticles by chilled and indirect sonication. (A−D) Cryo-TEM images of GMO/DOTAP/GMOPEG (95/4/1) aggregates displaying a number of colloidally stable spheroidal nanoparticles (average diameter of 500 nm) with internal bicontinuous cubic symmetry. The images clearly show that the PEGylated ternary lipid mixture when fragmented by sonication results in a cubosome-like particulate system with internal *Im3m* cubic structures mostly aligned in the (100) plane. (E−G) Cryo-TEM images of GMO/DOTAP/GMO-PEG (95/4/1)−siRNA complexes at $\rho = 1$. In this case, the particles display an analogous internal cubic structure, but the lighter water channels are now replaced with a much darker region, indicating that siRNA is encapsulated within the nanochannels. To our knowledge, this is the first time that a PEGylated cubosome including siRNA has been reported, and we name this material a "PEGylated cuboplex". (H) Schematic representation of the spherical PEGylated cuboplex particles with internal *Im3m* cubic structure. The gray surface represents the midplane of the lipid bilayer, and siRNA (illustrated as green helices) is included in the water channel domains; the PEG chains are represented as gray tails. (I) Magnified cryo-TEM image of the lipid-only *Im3m* cubosome and the corresponding FFT image showing that the particle is aligned in the (100) orientation, yielding a unit cell dimension of $a = 309$ Å. Note the dense outer rim in the cubosomes possibly resulting from a stabilizing PEGylated corona. (J) Magnified cryo-TEM of the lipid−siRNA *Im3m* cuboplex and FFT images showing alignment approximately in the (100) plane and $a = 169$ Å.

liposome, cryo-TEM has been extensively used to unequivocally demonstrate bicontinuous cubic structures of cubosomes and 2D hexagonal arrays of hexasomes.[67]

In Figure 3A−D, we can observe many individual particles in the 200 nm to 1 μm size range that have very well-ordered internal cubic structure obtained for a lipid composition of GMO/DOTAP/GMO-PEG (95/4/1). The internal structure is more clearly visible in Figure 3C,D. It is noteworthy that the nanoparticles are ordered in a specific direction, (100), through 2D mapping of the *Im3m* phase.[52] The cryo-TEM images of the lipid−siRNA cuboplexes at GMO/DOTAP/GMOPEG (95/4/1)−siRNA, ρ (n_{DOTAP}/n_{NA}) = 1, are displayed in Figure 3E−G. Figure 3H shows a schematic representation of the cuboplex nanoparticle with *Im3m* internal symmetry (gray minimal surface corresponding the lipid bilayer midplane) encapsulating siRNA (green helices). As opposed to lipid-only cubosomes, where one can easily observe light regions corresponding to the water channel domains, the cuboplexes appear darker and the internal structure is shrunk compared to lipid-only systems. The latter observation is consistent with the SAXS finding of a reduction of the cubic phase unit cell dimensions as siRNA is added to the cubosomes. siRNA is located at the water channel domain of the lipid-only cubosome system and is not surprising that those channels appear darker when siRNA is encapsulated. Figure 3I shows an expansion of a lipid-only cubosome image displaying the internal cubic symmetry aligned toward the (100) planes and the corresponding fast Fourier transforms (FFT) and Miller indices. The lattice constant was calculated from the FFT images,[68] yielding a unit cell of $a = 309$ Å for the lipid-only system, which is larger than that obtained by SAXS for the bulk phase ($a = 160$ Å). This indicates that

fragmentation of the bulk state gives rise to a particle where the structural cubic symmetry is conserved but with higher unit cell dimensions. An analogous expanded image obtained for siRNA-loaded cuboplexes is presented in Figure 3J with its corresponding FFT result. In this case, the internal cubic structure displays the *Im*3*m* symmetry as in the bulk phase with a unit cell dimension estimated by FFT of $a = 169$ Å, which is also larger than what is observed by SAXS ($a = 151$ Å). Consistent with the SAXS observations is that the unit cell of the lipid-only system is considerably reduced with the encapsulation of siRNA. The particulate system is obtained by a top-down approach, specifically by gentle indirect sonication of the bulk phase. It is natural that sonication induces molecular reorientations that would result in modulations of the lattice spacing. It is noteworthy that a dense outer membrane can be observed in the lipid-only cubosomes and in the siRNA-containing cuboplexes systems (cf. Figure 3E,J). At this point, we are not entirely sure what is the composition of the particle rims, but it is plausible that PEGylated lipids align preferentially at the surface of the particles, providing colloidal stabilization as seen for PEGylated liposomal systems. This would be particularly evident for the case when siRNA is associated within the internal water channels, displacing the PEGylated lipid components, and indeed, the rim on cuboplex particles appears denser and thicker compared to that in lipid-only cubosomes.

Gene Knockdown. We performed gene-silencing experiments to investigate the gene knockdown functionality of the new cuboplexes as carriers of exogenous siRNA as compared to classic liposomal siRNA formulations. The silencing efficiency as a measure of post-transcriptional, specific silencing of the gene targeted by the transferred siRNA of the cuboplexes was studied at different charge ratios (ρ) and compared to that of commercially available lipid-based complexes—*Lipofectamine* (LFA). In cell culture experiments, it is customary to employ complexes with excess positive charge ($\rho > 1$) in order to optimize their electrostatic affinity to negatively charged plasma membranes. In Figure S4, we show that the bicontinuous cubic structure of the complex is preserved at positive charge ratios. In one set of experiments, HeLa cells were pretreated to express firefly luciferase (FF), and thereafter, cuboplexes encapsulating siRNA targeting the FF luciferase mRNA for sequence-specific degradation were added to the cells. In this case, a control to off-target silencing effects was attained by incubating cells with cuboplexes encapsulating a "scramble" siRNA that has the same nucleotide composition, but not the same sequence, to test the effects of nonspecific gene knockdown. Figure 4A shows the luciferase activity in relative light units per milligram of protein following incubation of cells with LFA and cuboplexes at several charge ratios (ρ) represented by the green bars, in contrast to the "scramble" siRNA nonspecific knockdown activity plotted by the red bars. A control of the activity without any treatment (background signal from cells only) is represented by the "Neg" purple bar. Figure 4B shows the silencing activity results of an analogous experiment described above using lipid formulations, where the GMO neutral lipid was substituted by a classical liposomal-forming analogue species, DOPC (1,2-dioleoyl-*sn*-glycero-3-phosphocholine), and a phospholipid-based PEGylation agent (DOPE-PEG, 1,2-dioleoyl-*sn*-glycero-3-phosphoethanolamine-*N*-[methoxy(polyethylene glycol)-2000]). The molar fractions and charged densities were kept constant in both systems. The structures of the lipids used in the work can be consulted in Figure S5. A schematic representation of the type of lipid particle utilized as a starting point to incorporate siRNA in each experiment is included as an inset of Figure 4A (cubosomes) and Figure 4B (liposomes). A gray surface represents the midplane of a lipid bilayer, and a blue-shaded background represents the aqueous domains. In a liposome system, the lipid bilayer is a shell enveloping an isotropic aqueous interior as opposed to cubosomes, where a lipid bilayer folds into a bicontinuous cubic symmetry within the core of the particle interfacing a number of aqueous nanochannel domains.

There is not a systematic variation of the silencing efficiency with respect to ρ, but the best results are attained at $\rho = 3$ for the cuboplex system (75%). The liposome-based system does not allow for comparable gene knockdown efficacy (34%) unless significantly higher charge ratios of $\rho \geq 10$ are reached. Importantly, at this level, off-target silencing is extremely high. This is consistent with previous findings in our lab of bulk phases of lipid−siRNA complexes.[38,39] It should be noted that there is a strong correlation between high charge ratios (large excess of positive charges) to undesirable toxicity and concomitant off-target gene knockdown effects.[69] Interestingly, the cuboplexes give rise to gene-silencing functionalities at the very least comparable to the commercially available agent LFA and even 22% higher knockdown efficiency.

The silencing experiments described above are based on a pre-DNA transfection step that can lead to a number of issues interfering with the interpretation of the results. Namely, there can be a variation of DNA transfection efficiency propagating to siRNA delivery performances. In addition, there is a risk that endosomal uptake pathways become saturated with the first Lipofectamine dose (containing the DNA). In order to address this problem, we performed another set of experiments (Figure 4C,D) utilizing stably transfected luciferase reporter HeLa cell lines (HeLa-Luc). Figure 4C shows the luciferase activity in relative light units per milligram of protein following incubation of cells with cuboplexes at several charge ratios (ρ)

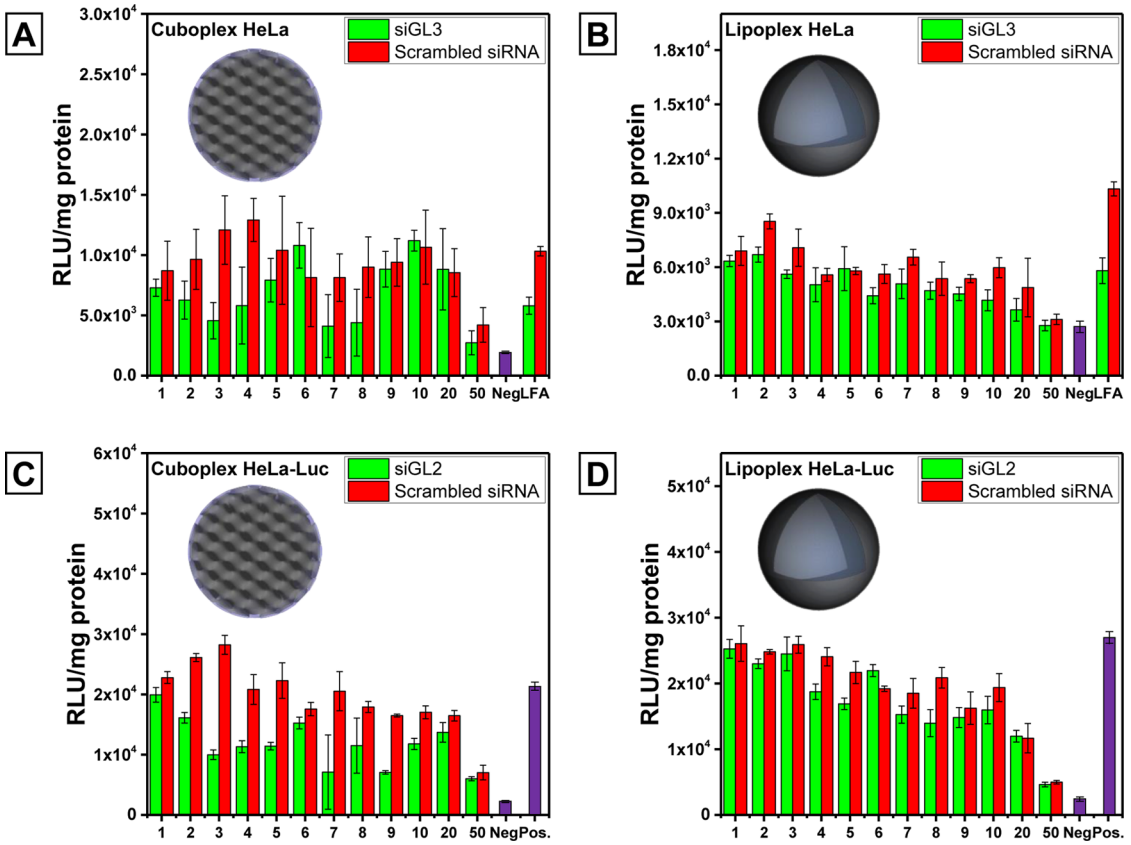

Figure 4. Luciferase gene knockdown in HeLa and HeLa-Luc cells of PEGylated GMO/DOTAP/GMO-PEG (95/4/1)–siRNA cuboplexes in contrast to liposome-based PEGylated DOPC/DOTAP/DOPE-PEG (95/4/1)–siRNA lipoplexes at different charge ratios (ρ). The schematics on the insets (A and C) represent the cubosome-based materials where the midplane of a lipid bilayer (gray surface) is folded within an aqueous interior of a particle (blue shade) having *Im3m* cubic symmetry. The liposome-based systems are schematically represented on the insets of B and D, where the lipid bilayer (gray surface) envelopes an isotropic aqueous interior (blue shade). As a reference knockdown product, a commercially available liposomal formulation (Lipofectamine, LFA) is also used. (A,B) HeLa cells were pretreated by transfection of plasmid DNA–firefly luciferase and subsequently incubated with either cuboplexes (A) or lipoplexes (B) containing two different siRNA (50 nM) molecules: siGL3 which targets the firefly luciferase mRNA to degrade and suppress expression (green bars) and "scramble" siRNA (red bars), which has random sequences to test nonspecific gene knockdown. "Neg" purple bars in the plots represent the signal obtained by cell-only without any treatment. In the regime of low ρ, where off-target effects are low, the Luciferase knockdown in HeLa cells with the cuboplex system is 75% *vs* 34% for the lipoplex ($\rho = 3$). Commercially available LFA is 53% efficient. (C,D) Luciferase gene knockdown in HeLa-Luc cells. The "Neg" purple bars in the plots represent a signal from wells with only cell media, and the "Pos" purple bars indicate signals from cells without any treatment. The Luciferase knockdown activity obtained with HeLa-Luc cells (siGL2, green bars) showed a behavior similar to that of HeLa cells, except that it displays smaller error bars. The efficiency of cuboplexes (C) in the low off-target (red bars) regime (low charge ratio ρ) is 70% *vs* 6% for the lipoplex system (D) at $\rho = 3$. The liposomal-based system can, at best, reach 38% efficiency (at $\rho = 8$), but at this point, off-target effects are already emerging. We suggest that these knockdown efficiency differences observed in both HeLa and HeLa-Luc cells are attributed to the fact that the bicontinuous cubic phase has membrane curvature characteristics that promote topological transformations of the endosomal membranes, such as facilitating pore formation, leading to efficient endosomal escape and concomitant efficient gene knockdown. In addition, the fact that there are minor nonspecific gene-silencing effects indicates that there should be no major toxicity issues associated with the cuboplex nanoparticles.

represented by the green bars, in contrast to the "scramble" siRNA nonspecific knockdown activity plotted by the red bars. Figure 4D shows the luciferase activity of a parent liposomal system. As a control, the "Neg" purple bar indicates signal from wells containing only cell media, and the "Pos" purple bars indicate background activity obtained from wells with cells only.

In general, the knockdown behavior as a function of ρ is very similar to that obtained with pretransfected HeLa cells (Figure 4A,B). It is noteworthy that all cell culture results reported are an average of at least three independent cell culture experiments at different days. In addition, each measurement is recorded at least in triplicate. In the case of the silencing activity obtained with the Hela-Luc cells (Figure 4C,D), there is considerably less variation in the results when compared to the pretransfected Hela cells. The gene-silencing activities attained with the cuboplex (Figure 4C) are clearly more favorable (without significant off-target effects) than what is obtained with the parent liposome-based system (Figure 4D) at all charge ratios. At as low as $\rho = 3$, the efficiency of the cuboplex is 70% *vs* 6% for the liposome-based carrier. At best, when $\rho = 8$, the

liposomal system reaches 38% knockdown efficiency, but off-target effects start to emerge at this regime of high charge ratios. We should note that the lipids utilized in the liposomal formulation are standard phospholipids used in many drug and nucleic acid delivery applications. The absolute silencing efficacy of the cuboplexes is encouraging *per se* while establishing a new handle for future lipid-based siRNA delivery systems that so far have not explored the importance of membrane structures that deviate from the classical liposome design.

Considering Helfrich membrane elasticity arguments,[70] a bicontinuous cubic phase, as presented in the cuboplexes, should have efficient fusogenic properties independent of membrane charge density. The elastic energy per unit area (E/A) of a lipid bilayer membrane of spontaneous zero mean curvature ($C_0 = 0$) is given by $E/A = 0.5\kappa C^2 + \kappa_G C_1 C_2$, where C_1 and C_2 are the principal curvatures of the membrane aggregate, and κ and κ_G are the bending and Gaussian modulus, respectively. The first term represents the energetic cost of bending a membrane away from its spontaneous curvature C_0, and the second term accounts for membrane topology changes. For membranes with a negative Gaussian modulus, $\kappa_G < 0$, spherically shaped vesicles with positive curvature $C_1C_2 > 0$ are favored. On the other hand, membranes with a positive Gaussian modulus, $\kappa_G > 0$, will favor saddle-splay-shaped surfaces with negative Gaussian curvature $C_1C_2 < 0$ such as the surfaces of bicontinuous cubic phases (cf. Figure 2D). Cubic-phase-forming lipids ($\kappa_G > 0$) should give rise to enhanced membrane fusion, which requires the spontaneous transient formation of pores that also have negative Gaussian curvature surfaces. In fact, membrane fusion mediated by pore formation has been mechanistically associated with the stabilization of bicontinuous cubic phases.[71,72] We attribute the high silencing efficiency results to the ability of the cuboplexes to lower the free energy cost of fusion and concomitant pore formation between the membranes of the cuboplex and the endosome. Interestingly, the inclusion of PEGylated moieties that is traditionally known to compromise the efficiency of exogenous nucleic acid cellular delivery due to surface charge alteration effects[73] does not seem to diminish the functionalities of the cuboplexes. This finding further indicates that the mechanism of siRNA cell entry does not rely on electrostatic attachments between complexes and endosomal membranes, and it is rather a membrane topologically activated mechanism.

CONCLUSIONS

In this work, we demonstrate that the internal structure of particles has a determining role in their efficiency as carriers for cellular delivery. Specifically, we developed a method to stabilize lipid-based dispersions with remarkably ordered internal bicontinuous cubic symmetry (*Im*3*m* space group) that is able to encapsulate large amounts of siRNA even at very low membrane positive charge density. The bicontinuous cubic structure is topologically active, being able to efficiently escape endosomal entrapment by lowering the free energy cost of forming pores in endosomal membranes, leading to efficient siRNA delivery to the cell. The efficiency of this new lipid-based material surpasses that of parent liposome-based systems as well as commercially available products for siRNA delivery. Furthermore, the particles with internal cubic structure are sterically stabilized by lipids conjugated with polyethylene glycol (PEG) moieties, allowing them to be used in systemic delivery. This is the first time that a PEGylated lipid particle with internal cubic symmetry containing siRNA is reported, and we name these new particles *PEGylated cuboplexes*. The particles are produced by gentle, indirect, and chilled sonication based on a tricomponent system made of glycerol monooleate (a lipid that has a tendency to form cubic phases), a positively charged lipid to electrostatically entrap siRNA (1,2-dioleoyl-3-trimethylammonium propane), and GMO covalently linked to a 2 kDa PEG unit that provides colloidal and steric stability. The incorporation of very small amounts of GMO-PEG has a dramatic effect on the DOTAP/GMO phase behavior, leading to transformations between bicontinuous cubic phases of different symmetry groups (*Im*3*m* stable at 1 mol % of GMO-PEG and *Ia*3*d* at 2 mol %). Furthermore, the content of GMO-PEG offers an alternative handle (in addition to reported charged lipids and/or cholesterol) to control unit cell dimensions of the bicontinuous cubic phases with an increase in lattice spacing of the gyroid phase *Ia*3*d* from 217 Å at $\Phi_{GMO\text{-}PEG} = 0.02$ to 245 Å at $\Phi_{GMO\text{-}PEG} = 0.03$ and eventually 313 Å at $\Phi_{GMO\text{-}PEG} = 0.04$. siRNA can be encapsulated with an efficiency of 90% without disruption of the topology of the PEGylated cubic phase only for the *Im*3*m* symmetry group (while the *Ia*3*d* gyroid is converted fully to a 2D reversed hexagonal phase). Even though both bicontinuous cubic phases have analogous genus, *Im*3*m* has a lower surface area compared to that of *Ia*3*d* and concomitant larger regions of flatter lipid membranes, which present a more stable state to accommodate stiff nucleic acid molecules such as siRNA. Upon passive siRNA encapsulation, the colloidally stable cubosomes with *ca.* 500 nm diameter and well-ordered internal *Im*3*m* cubic structure are conserved, resulting in cuboplex particles of the same size but with unit cell reductions consistent with siRNA-induced screening of cationic lipid electrostatic repulsion. In addition, cryo-TEM imaging shows that the water channel domains in the lipid-only cubosomes are clearly filled with siRNA in the siRNA-containing cuboplex. Remarkably, knockdown efficiency is not compromised by the addition of PEG units to the particles, indicating that the

mechanism of endosomal escape is not limited or controlled by electrostatic interactions as classically obtained for siRNA delivery carriers, but it is instead reliant on topologically activated processes that are completely dictated by the internal structures of the particles.

METHODS

Preparation of Lipid−siRNA Complexes. The lipid components utilized were GMO, purchased from NU-CHECK PREP Inc. (Elysian), 1,2-dioleoyl-3-trimethylammonium-propane, 1,2-dioleoyl-*sn*-glycero-3-phosphocholine, and 1,2-dioleoyl-*sn*-glycero-3-phosphoethanolamine-*N*-[methoxy(polyethylene glycol)-2000] obtained from Avanti Polar Lipids, Inc. (Alabaster), and PEG-conjugated GMO that was custom-designed by NOF America Corporation (White Plains). The chemical structure of these lipids can be consulted in Figure S5. All lipids were used without further purification and dissolved in chloroform, combining the solutions at the desired volumetric ratios and evaporating the solvent, first under a stream of nitrogen and then in a vacuum overnight. The resulting lipid film was hydrated at 37 °C for 2 days with sterile water (18.2 MΩ·cm) from a Milli-Q filtration system (Millipore, Germany) or an RNase free water for the lipid−siRNA complex. The final lipid concentration was 500 mM (for SAXS), 10 mM (for cell culture studies), and 1 mM (for dilute cryo-TEM samples). siRNA (19 base pair, CUUACGCUGAGUACUUCGA with two 3′-deoxythymidine overhangs, from Dharmacon (Germany), at 10 μg/μL that specifically targets the firefly luciferase gene) was added in the hydration step at the desired charge ratio ρ (n_{DOTAP}/n_{NA}) for cryo-TEM samples. Cubosomes (lipid-only) and cuboplexes (lipid−siRNA complexes) were prepared by indirect sonication using a cup horn system (Qsonica) with temperature control below 4 °C (Fisher Scientific) for 6 min. During the sonication, the ultrasound frequency was 20 kHz, the amplitude was kept for 100%, and the average power applied to the system was 700 W. For the lipid−siRNA complex samples used in SAXS, the prepared lipid solution (50 mM) was mixed with siRNA with the desired ratio ρ using a table-top centrifuge at 4 °C for 15 min.

Small-Angle X-ray Scattering. Lipid and lipid−siRNA complexes were prepared in quartz capillaries (Hilgenberg Glas, Germany). SAXS experiments were conducted in a home-built (with help of Forvis Technologies, Santa Barbara, CA, USA) equipment composed of a Xenocs GeniX3D Cu Kα ultralow divergence X-ray source (1.54 Å/8 keV), with a divergence of ∼1.3 mrad. The 2D diffraction data were radially averaged upon acquisition on a Pilatus 300 K 20 Hz hybrid pixel detector (Dectris) and integrated using FIT2D software (http://www.esrf.eu/computing/scientific/FIT2D) from ESRF.[74,75]

Confocal Microscopy. The lipid−siRNA complex samples for confocal microscopy (Leica SP2 visible laser confocal microscope, Leica Microsystems) were prepared by mixing red fluorescent dye (0.1 mol % of Texas Red DHPE, Lifetechnologies) tagged lipid solutions with siRNA labeled (green fluorescent dye at one dye molecule per 15 bp, YoYo-1 iodide, Molecular Probes) at ρ = 1. The concentrations of lipid and siRNA stock solutions were 1 mM and 1 mg/mL, respectively.

Cryogenic Transmission Electron Microscopy. Lipid and lipid−siRNA complex samples for cryogenic transmission electron microscopy (JEOL 2100 cryo-TEM at 120 kV) were prepared on a lacey carbon-coated copper grid (Structure Probe Incorporation, PA) using semiautomated Vitrobot (Vitrobot Mark II, FEI). Briefly, 1 μL of 1 mM cubosome or cuboplex solution was casted on top of a carbon grid. The grid was then transferred to Vitrobot chamber that was at 100% humidity and at 4 °C. Rapid immersion of the grid into liquid ethane after 1 s blotting effectively vitrifies the sample. Note that the samples should be kept under −170 °C until successfully transferred into the cryo-TEM instrument in order to prevent crystalline ice formation. The images are obtained at a defocus of ∼4000 nm.

Cell Culture and Gene Knockdown. Human tumor cells (HeLa, CCL-2 by ATCC) and stable overexpressing luciferase HeLa cells (HeLa-Luc, SL-0102 by Signosis) were cultured in Dulbecco's modified Eagle's medium (mixture of 10% fetal bovine serum and 1% penicillin-streptomycin) at 37 °C with 5% of carbon dioxide (CO_2). The siRNA knockdown experiments with HeLa cells were done by the method described as follows. First 0.1 μg of plasmid DNA (pGL3 firefly, Promega) was transfected using Lipofectamine 2000 (L2000, Invitrogen) by incubating HeLa cells for at least 2 h at approximately 10 000 cells seeded per well in a 96-well plate. After DNA transfection, HeLa cells were washed with fresh PBS (1×, Corning). HeLa cells were then incubated with 50 nM "scrambled" siRNA (Allstars negative control siRNA, QIAGEN) or 50 nM siRNA targeting firefly luciferase genes per well at different charge ratios (ρ) for more than 2 h. The siRNA knockdown experiments with HeLa-Luc cells were done in an analogous way utilizing 50 nM of luciferase targeting siRNA, siGL2 (Dharmacon), and a scrambled siRNA to test for off-target effects. The main difference in these experiments is that the pretransfection step with DNA is not required as this cell line naturally expresses luciferase mRNA. Gene knockdown efficiency was then evaluated using the luciferase assay system (Promega, USA). Specifically, the produced light from each well of interest was measured by a plate reader (Victor 3 multilabel reader, PerkinElmer) and normalized by the mass of cells in each well. Each reported result is a result of three independent cell culture experiments performed on different days. In addition, each well during one experiment is conducted in triplicate.

Conflict of Interest: The authors declare no competing financial interest.

Supporting Information Available: The Supporting Information is available free of charge on the ACS Publications website at DOI: 10.1021/acsnano.5b03902.

Figures S1−S5 and Table S1 (PDF)

Acknowledgment. This work was supported by the Campus Research Board and start-up funding from the University of Illinois at Urbana—Champaign, College of Engineering (Materials Science and Engineering and Materials Research Laboratory). We would like to thank Dr. Nathan Gabrielson for his assistance with cell culture experiments.

REFERENCES AND NOTES

1. Peer, D.; Karp, J. M.; Hong, S.; Farokhzad, O. C.; Margalit, R.; Langer, R. Nanocarriers as an Emerging Platform for Cancer Therapy. *Nat. Nanotechnol.* **2007**, *2*, 751–760.
2. Davis, M. E.; Chen, Z.; Shin, D. M. Nanoparticle Therapeutics: an Emerging Treatment Modality for Cancer. *Nat. Rev. Drug Discovery* **2008**, *7*, 771–782.
3. Jain, R. K.; Stylianopoulos, T. Delivering Nanomedicine to Solid Tumors. *Nat. Rev. Clin. Oncol.* **2010**, *7*, 653–664.
4. Petros, R. A.; DeSimone, J. M. Strategies in the Design of Nanoparticles for Therapeutic Applications. *Nat. Rev. Drug Discovery* **2010**, *9*, 615–627.
5. Cabral, H.; Matsumoto, Y.; Mizuno, K.; Chen, Q.; Murakami, M.; Kimura, M.; Terada, Y.; Kano, M. R.; Miyazono, K.; Uesaka, M.; et al. Accumulation of Sub-100 nm Polymeric Micelles in Poorly Permeable Tumours Depends on Size. *Nat. Nanotechnol.* **2011**, *6*, 815–823.
6. Jiang, W.; Kim, B. Y. S.; Rutka, J. T.; Chan, W. C. W. Nanoparticle-mediated Cellular Response is Size-Dependent. *Nat. Nanotechnol.* **2008**, *3*, 145–150.
7. Reddy, S. T.; van der Vlies, A. J.; Simeoni, E.; Angeli, V.; Randolph, G. J.; O'Neil, C. P.; Lee, L. K.; Swartz, M. A.; Hubbell, J. A. Exploiting Lymphatic Transport and Complement Activation in Nanoparticle Vaccines. *Nat. Biotechnol.* **2007**, *25*, 1159–1164.
8. Tang, L.; Yang, X.; Yin, Q.; Cai, K.; Wang, H.; Chaudhury, I.; Yao, C.; Zhou, Q.; Kwon, M.; Hartman, J. A.; et al.

Investigating the Optimal Size of Anticancer Nanomedicine. *Proc. Natl. Acad. Sci. U. S. A.* **2014**, *111*, 15344–15349.
9. Barua, S.; Mitragotri, S. Challenges Associated with Penetration of Nanoparticles Across Cell and Tissue Barriers: A Review of Current Status and Future Prospects. *Nano Today* **2014**, *9*, 223–243.
10. Yoo, J.-W.; Irvine, D. J.; Discher, D. E.; Mitragotri, S. Bio-inspired, Bioengineered and Biomimetic Drug Delivery Carriers. *Nat. Rev. Drug Discovery* **2011**, *10*, 521–535.
11. Jadhao, V.; Thomas, C. K.; Olvera de la Cruz, M. Electrostatics-Driven Shape Transitions in Soft Shells. *Proc. Natl. Acad. Sci. U. S. A.* **2014**, *111*, 12673–12678.
12. Yao, Z.; Sknepnek, R.; Thomas, C. K.; Olvera de la Cruz, M. Shapes of Pored Membranes. *Soft Matter* **2012**, *8*, 11613–11619.
13. Perry, J. L.; Herlihy, K. P.; Napier, M. E.; Desimone, J. M. PRINT: A Novel Platform toward Shape and Size Specific Nanoparticle Theranostics. *Acc. Chem. Res.* **2011**, *44*, 990–998.
14. Barua, S.; Mitragotri, S. Synergistic Targeting of Cell Membrane, Cytoplasm, and Nucleus of Cancer Cells Using Rod-Shaped Nanoparticles. *ACS Nano* **2013**, *7*, 9558–9570.
15. Leung, C.-Y.; Palmer, L. C.; Qiao, B. F.; Kewalramani, S.; Sknepnek, R.; Newcomb, C. J.; Greenfield, M. A.; Vernizzi, G.; Stupp, S. I.; Bedzyk, M. J.; et al. Molecular Crystallization Controlled by pH Regulates Mesoscopic Membrane Morphology. *ACS Nano* **2012**, *6*, 10901–10909.
16. Vernizzi, G.; Sknepnek, R.; Olvera de la Cruz, M. Platonic and Archimedean Geometries in Multicomponent Elastic Membranes. *Proc. Natl. Acad. Sci. U. S. A.* **2011**, *108*, 4292–4296.
17. Sing, C. E.; Zwanikken, J. W.; Olvera de la Cruz, M. Electrostatic Control of Block Copolymer Morphology. *Nat. Mater.* **2014**, *13*, 694–698.
18. Fire, A.; Xu, S. Q.; Montgomery, M. K.; Kostas, S. A.; Driver, S. E.; Mello, C. C. Potent and Specific Genetic Interference by Double-Stranded RNA in Caenorhabditis Elegans. *Nature* **1998**, *391*, 806–811.
19. Elbashir, S. M.; Harborth, J.; Lendeckel, W.; Yalcin, A.; Weber, K.; Tuschl, T. Duplexes of 21-Nucleotide RNAs Mediate RNA interference in Cultured Mammalian Cells. *Nature* **2001**, *411*, 494–498.
20. Yin, H.; Kanasty, R. L.; Eltoukhy, A. A.; Vegas, A. J.; Dorkin, J. R.; Anderson, D. G. Non-Viral Vectors for Gene-based Therapy. *Nat. Rev. Genet.* **2014**, *15*, 541–555.
21. Whitehead, K. A.; Dorkin, J. R.; Vegas, A. J.; Chang, P. H.; Veiseh, O.; Matthews, J.; Fenton, O. S.; Zhang, Y.; Olejnik, K. T.; Yesilyurt, V.; et al. Degradable Lipid Nanoparticles with Predictable *in Vivo* siRNA Delivery Activity. *Nat. Commun.* **2014**, *5*, 4277.
22. Bouchie, A. Companies in Footrace to Deliver RNAi. *Nat. Biotechnol.* **2012**, *30*, 1154–1157.
23. Thi, E. P.; Mire, C. E.; Lee, A. C. H.; Geisbert, J. B.; Zhou, J. Z.; Agans, K. N.; Snead, N. M.; Deer, D. J.; Barnard, T. R.; Fenton, K. A.; et al. Lipid Nanoparticle siRNA Treatment of Ebola-Virus-Makona-infected Nonhuman Primates. *Nature* **2015**, *521*, 362–365.
24. Davis, M. E.; Zuckerman, J. E.; Choi, C. H. J.; Seligson, D.; Tolcher, A.; Alabi, C. A.; Yen, Y.; Heidel, J. D.; Ribas, A. Evidence of RNAi in Humans from Systemically Administered siRNA *via* Targeted Nanoparticles. *Nature* **2010**, *464*, 1067–1070.
25. Semple, S. C.; Akinc, A.; Chen, J.; Sandhu, A. P.; Mui, B. L.; Cho, C. K.; Sah, D. W. Y.; Stebbing, D.; Crosley, E. J.; Yaworski, E.; et al. Rational Design of Cationic Lipids for siRNA Delivery. *Nat. Biotechnol.* **2010**, *28*, 172–176.
26. Novobrantseva, T. I.; Borodovsky, A.; Wong, J.; Klebanov, B.; Zafari, M.; Yucius, K.; Querbes, W.; Ge, P.; Ruda, V. M.; Milstein, S.; et al. Systemic RNAi-Mediated Gene Silencing in Nonhuman Primate and Rodent Myeloid Cells. *Mol. Ther.--Nucleic Acids* **2012**, *1*, e4.
27. Rozema, D. B.; Lewis, D. L.; Wakefield, D. H.; Wong, S. C.; Klein, J. J.; Roesch, P. L.; Bertin, S. L.; Reppen, T. W.; Chu, Q.; Blokhin, A. V.; et al. Dynamic PolyConjugates for Targeted *in Vivo* Delivery of siRNA to Hepatocytes. *Proc. Natl. Acad. Sci. U. S. A.* **2007**, *104*, 12982–12987.
28. Kanasty, R.; Dorkin, J. R.; Vegas, A.; Anderson, D. Delivery Materials for siRNA Therapeutics. *Nat. Mater.* **2013**, *12*, 967–977.
29. Garber, K. Biotech in a Blink. *Nat. Biotechnol.* **2010**, *28*, 311–314.
30. Wang, A. Z.; Langer, R.; Farokhzad, O. C. Nanoparticle Delivery of Cancer Drugs. *Annu. Rev. Med.* **2012**, *63*, 185–198.
31. Lin, A. J.; Slack, N. L.; Ahmad, A.; George, C. X.; Samuel, C. E.; Safinya, C. R. Three-Dimensional Imaging of Lipid Gene-Carriers: Membrane Charge Density Controls Universal Transfection Behavior in Lamellar Cationic Liposome-DNA Complexes. *Biophys. J.* **2003**, *84*, 3307–3316.
32. Zuckerman, J. E.; Choi, C. H. J.; Han, H.; Davis, M. E. Polycation-siRNA Nanoparticles Can Disassemble at the Kidney Glomerular Basement Membrane. *Proc. Natl. Acad. Sci. U. S. A.* **2012**, *109*, 3137–3142.
33. Naeye, B.; Deschout, H.; Caveliers, V.; Descamps, B.; Braeckmans, K.; Vanhove, C.; Demeester, J.; Lahoutte, T.; De Smedt, S. C.; Raemdonck, K. *In Vivo* Disassembly of IV Administered siRNA Matrix Nanoparticles at the Renal Filtration Barrier. *Biomaterials* **2013**, *34*, 2350–2358.
34. Yuan, F.; Leunig, M.; Huang, S. K.; Berk, D. A.; Papahadjopoulos, D.; Jain, R. K. Mirovascular Permeability and Interstitial Penetration of Sterically Stabilized (Stealth) Liposomes in a Human Tumor Xenograft. *Cancer Res.* **1994**, *54*, 3352–3356.
35. Awasthi, V. D.; Garcia, D.; Goins, B. A.; Phillips, W. T. Circulation and Biodistribution Profiles of Long-Circulating PEG-liposomes of Various Sizes in Rabbits. *Int. J. Pharm.* **2003**, *253*, 121–132.
36. Yu, B.; Zhao, X.; Lee, L. J.; Lee, R. J. Targeted Delivery Systems for Oligonucleotide Therapeutics. *AAPS J.* **2009**, *11*, 195–203.
37. Sahay, G.; Querbes, W.; Alabi, C.; Eltoukhy, A.; Sarkar, S.; Zurenko, C.; Karagiannis, E.; Love, K.; Chen, D.; Zoncu, R.; et al. Efficiency of siRNA Delivery by Lipid Nanoparticles Is Limited by Endocytic Recycling. *Nat. Biotechnol.* **2013**, *31*, 653–658.
38. Leal, C.; Bouxsein, N. F.; Ewert, K. K.; Safinya, C. R. Highly Efficient Gene Silencing Activity of siRNA Embedded in a Nanostructured Gyroid Cubic Lipid Matrix. *J. Am. Chem. Soc.* **2010**, *132*, 16841–16847.
39. Leal, C.; Ewert, K. K.; Shirazi, R. S.; Bouxsein, N. F.; Safinya, C. R. Nanogyroids Incorporating Multivalent Lipids: Enhanced Membrane Charge Density and Pore Forming Ability for Gene Silencing. *Langmuir* **2011**, *27*, 7691–7697.
40. Kang, M.; Huang, G.; Leal, C. Role of Lipid Polymorphism in Acoustically Sensitive Liposomes. *Soft Matter* **2014**, *10*, 8846–8854.
41. Simberg, D.; Hirsch-Lerner, D.; Nissim, R.; Barenholz, Y. Comparison of Different Commercially Available Cationic Lipid Based Transfection Kits. *J. Liposome Res.* **2000**, *10*, 1–13.
42. Angelov, B.; Angelova, A.; Papahadjopoulos-Sternberg, B.; Hoffmann, S. V.; Nicolas, V.; Lesieur, S. Protein-Containing PEGylated Cubosomic Particles: Freeze-Fracture Electron Microscopy and Synchrotron Radiation Circular Dichroism Study. *J. Phys. Chem. B* **2012**, *116*, 7676–7686.
43. Larsson, K. Cubic Lipid-Water Phases: Structures and Biomembrane Aspects. *J. Phys. Chem.* **1989**, *93*, 7304–7314.
44. Barauskas, J.; Johnsson, M.; Joabsson, F.; Tiberg, F. Cubic Phase Nanoparticles (Cubosome†): Principles for Controlling Size, Structure, and Stability. *Langmuir* **2005**, *21*, 2569–2577.
45. Johnsson, M.; Barauskas, J.; Tiberg, F. Cubic Phases and Cubic Phase Dispersions in a Phospholipid-Based System. *J. Am. Chem. Soc.* **2005**, *127*, 1076–1077.
46. Murgia, S.; Bonacchi, S.; Falchi, A. M.; Lampis, S.; Lippolis, V.; Meli, V.; Monduzzi, M.; Prodi, L.; Schmidt, J.; Talmon, Y.; et al. Drug-Loaded Fluorescent Cubosomes: Versatile Nanoparticles for Potential Theranostic Applications. *Langmuir* **2013**, *29*, 6673–6679.

47. Guillot, S.; Salentinig, S.; Chemelli, A.; Sagalowicz, L.; Leser, M. E.; Glatter, O. Influence of the Stabilizer Concentration on the Internal Liquid Crystalline Order and the Size of Oil-Loaded Monolinolein-Based Dispersions. *Langmuir* **2010**, *26*, 6222–6229.
48. Mulet, X.; Gong, X.; Waddington, L. J.; Drummond, C. J. Observing Self-Assembled Lipid Nanoparticles Building Order and Complexity through Low-Energy Transformation Processes. *ACS Nano* **2009**, *3*, 2789–2797.
49. Angelov, B.; Angelova, A.; Papahadjopoulos-Sternberg, B.; Lesieur, S.; Sadoc, J.-F.; Ollivon, M.; Couvreur, P. Detailed Structure of Diamond-Type Lipid Cubic Nanoparticles. *J. Am. Chem. Soc.* **2006**, *128*, 5813–5817.
50. Marrink, S.-J.; Tieleman, D. P. Molecular Dynamics Simulation of a Lipid Diamond Cubic Phase. *J. Am. Chem. Soc.* **2001**, *123*, 12383–12391.
51. Nakano, M.; Sugita, A.; Matsuoka, H.; Handa, T. Small-Angle X-ray Scattering and 13C NMR Investigation on the Internal Structure of "Cubosomes. *Langmuir* **2001**, *17*, 3917–3922.
52. Gustafsson, J.; Ljusberg-Wahren, H.; Almgren, M.; Larsson, K. Cubic Lipid−Water Phase Dispersed into Submicron Particles. *Langmuir* **1996**, *12*, 4611–4613.
53. Martiel, I.; Sagalowicz, L.; Handschin, S.; Mezzenga, R. Facile Dispersion and Control of Internal Structure in Lyotropic Liquid Crystalline Particles by Auxiliary Solvent Evaporation. *Langmuir* **2014**, *30*, 14452–14459.
54. Hahn, T. *International Tables for Crystallography*, 3rd revised ed.; Kluwer Academic: Dordrecht, The Netherlands, 1992; Vol. A, space-group symmetry.
55. Larsson, K. Two Cubic Phases in Monoolein-Water System. *Nature* **1983**, *304*, 664–665.
56. Gupta, A.; Stait-Gardner, T.; de Campo, L.; Waddington, L. J.; Kirby, N.; Price, W. S.; Moghaddam, M. J. Nanoassemblies of Gd−DTPA−Monooleyl and Glycerol Monooleate Amphiphiles as Potential MRI Contrast Agents. *J. Mater. Chem. B* **2014**, *2*, 1225–1233.
57. Engblom, J.; Miezis, Y.; Nylander, T.; Razumas, V.; Larsson, K. On the Swelling of Monoolein Liquid-Crystalline Aqueous Phases in the Presence of Distearoylphosphatidylglycerol. *Prog. Colloid Polym. Sci.* **2001**, *116*, 9–15.
58. Tyler, A. I. I.; Barriga, H. M. G.; Parsons, E. S.; McCarthy, N. L. C.; Ces, O.; Law, R. V.; Seddon, J. M.; Brooks, N. J. Electrostatic Swelling of Bicontinuous Cubic Lipid Phases. *Soft Matter* **2015**, *11*, 3279–3286.
59. Seddon, J. M.; Templer, R. H. Polymorphism of Lipid−Water Systems. In *Handbook of Biological Physics*; Lipowsky, R., Sackmann, E., Eds.; Elsevier: North-Holland, The Netherlands, 1995; Vol. 1, pp 97−160.
60. Rädler, J. O.; Koltover, I.; Salditt, T.; Safinya, C. R. Structure of DNA-Cationic Liposome Complexes: DNA Intercalation in Multilamellar Membranes in Distinct Interhelical Packing Regimes. *Science* **1997**, *275*, 810–814.
61. Leal, C.; Ewert, K. K.; Bouxsein, N. F.; Shirazi, R. S.; Li, Y.; Safinya, C. R. Stacking of Short DNA Induces the Gyroid Cubic-to-Inverted Hexagonal Phase Transition in Lipid DNA Complexes. *Soft Matter* **2013**, *9*, 795–804.
62. Zhen, G.; Hinton, T. M.; Muir, B. W.; Shi, S.; Tizard, M.; McLean, K. M.; Hartley, P. G.; Gunatillake, P. Glycerol Monooleate-Based Nanocarriers for siRNA Delivery *in Vitro*. *Mol. Pharmaceutics* **2012**, *9*, 2450–2457.
63. Cherezov, V.; Clogston, J.; Misquitta, Y.; Abdel-Gawad, W.; Caffrey, M. Membrane Protein Crystallization In Meso: Lipid Type-Tailoring of the Cubic Phase. *Biophys. J.* **2002**, *83*, 3393–3407.
64. Chiu, M. L.; Nollert, P.; Loewen, M. C.; Belrhali, H.; Pebay-Peyroula, E.; Rosenbusch, J. P.; Landau, E. M. Crystallization in Cubo: General Applicability to Membrane Proteins. *Acta Crystallogr., Sect. D: Biol. Crystallogr.* **2000**, *56*, 781–784.
65. Qiu, H.; Caffrey, M. Lyotropic and Thermotropic Phase Behavior of Hydrated Monoacylglycerols: Structure Characterization of Monovaccenin. *J. Phys. Chem. B* **1998**, *102*, 4819–4829.
66. Crawford, R.; Dogdas, B.; Keough, E.; Haas, R. M.; Wepukhulu, W.; Krotzer, S.; Burke, P. A.; Sepp-Lorenzino, L.; Bagchi, A.; Howell, B. J. Analysis of Lipid Nanoparticles by Cryo-EM for Characterizing siRNA Delivery Vehicles. *Int. J. Pharm.* **2011**, *403*, 237–244.
67. Almgren, M.; Edwards, K.; Karlsson, G. Cryo Transmission Electron Microscopy of Liposomes and Related structures. *Colloids Surf., A* **2000**, *174*, 3–21.
68. Sagalowicz, L.; Michel, M.; Adrian, M.; Frossard, P.; Rouvet, M.; Watzke, H. J.; Yaghmur, A.; De Campo, L.; Glatter, O.; Leser, M. E. Crystallography of Dispersed Liquid Crystalline Phases Studied by Cryo-Transmission Electron Microscopy. *J. Microsc.* **2006**, *221*, 110–121.
69. Bouxsein, N. F.; McAllister, C. S.; Ewert, K.; Samuel, C. E.; Safinya, C. R. Structure and Gene Silencing Activities of Monovalent and Pentavalent Cationic Lipid Vectors Complexed with siRNA. *Biochemistry* **2007**, *46*, 4785–4792.
70. Helfrich, W. Z. Elastic Properties of Lipid Bilayers - Theory and Possible Experiments. *Z. Naturforsch.* **1973**, *C28*, 693–703.
71. Porte, G. Lamellar Phases and Disordered Phases of Fluid Bilayer Membranes. *J. Phys.: Condens. Matter* **1992**, *4*, 8649–8670.
72. Siegel, D. P.; Epand, R. M. The Mechanism of Lamellar-to-Inverted Hexagonal Phase Transitions in Phosphatidylethanolamine: Implications for Membrane Fusion Mechanisms. *Biophys. J.* **1997**, *73*, 3089–3111.
73. Majzoub, R. N.; Chan, C.-L.; Ewert, K. K.; Silva, B. F. B.; Liang, K. S.; Jacovetty, E. L.; Carragher, B.; Potter, C. S.; Safinya, C. R. Uptake and Transfection Efficiency of PEGylated Cationic Liposome−DNA Complexes with and without RGD-tagging. *Biomaterials* **2014**, *35*, 4996–5005.
74. Hammersley, A. P.; Svensson, S. O.; Hanfland, M.; Fitch, A. N.; Hausermann, D. Two-Dimensional Detector Software: From Real Detector to Idealised Image or Two-Theta Scan. *High Pressure Res.* **1996**, *14*, 235–248.
75. Hammersley, A. P. ESRF Internal Report 1998, ESRF98HA01T, FIT2D V9.129 reference manual V3.1, **1998**.